Zahra Jlassi[1,*], Khadija Ben Kilani[1], Mohamed Elleuch[1], Lamine Mili[2]

J. Electrical Systems 16-1 (2020): 1-15

Regular paper

A Combined Koopman-Subgraph Method for a Secure Power System Islanding

Journal of Electrical Systems

This paper proposes a new methodology for power system islanding based on Koopman modal coherency (KMC) combined with subgraph theory. Initial system partitioning is determined from the Koopman bus-angle coherency matrix. Then, the technique of subgraph is used to modulate the partitions, yielding to viable islands. Balancing subgraphs are constructed from the clusters pairwise neighboring areas. Overload subgraphs swap to connected over-generation subgraphs. Stable islands satisfy nonlinear dynamic coherency, and minimal power mismatch. The search algorithm substantiates the required bands specified in the frequency operating standards. Under severe disturbances, over-frequency generation shedding and under-frequency load shedding schemes are implemented. The proposed islanding methodology is demonstrated on a realistic 151-bus, 24-machines power system. Results show that the proposed scheme can reduce failure regions in faulted power systems.

Keywords: Power system; Koopman modes analysis; Controlled islanding; Coherency; Subgraph.
Article history: Received 17 May 2019, Accepted 12 December 2019

1. Introduction

Islanding in a power system is a relatively rare event, undertaken by system operators under unfavorable emergency operating conditions [1]-[3]. It aims at splitting the system into islanded subsystems following cascading failures originating from a localized disturbance, hence confining system breakdown over a limited area. In order for the islands that do not breakdown to continue operating, two main viability conditions are compulsory: (i) coherency among generators and bus clusters, and (ii) satisfaction of the minimum threshold constraints for generation-load mismatch, voltage deviation and transmission lines loadability.

A wide range of methodologies for coherency identification and bus clustering techniques has been proposed in the literature. The approaches underlying these techniques differ in input models or data and the coherency search scheme. Largely, they may be classified as model-based and measurement-based, or alternatively as static and dynamic methods, as summarized in Table 1. Model-based techniques include time simulations [4], energy based techniques [5], and slow coherency [6], [7]. Measurement-based coherency identification techniques include artificial neural networks (ANN) [8], [9], principal component analysis (PCA) [10], particle swarm optimization (PSO) [11], Hilbert- Huang

Table 1: Classification of Coherency Search Methods

Input data \ Method	Visual testing	Energy based	Modal Analysis	Graph Theory	Intelligent computation
Equations	Time simulation	Energy functions	Slow-coherency	Weak connections	
Measurements			Koopman Modal	Spectral- graph	ANN, PCA, PSO, HHT, SOM…

[*] Corresponding author: Z. Jlassi, ENIT-L.S.E-LR11ES15, University of Tunis EL Manar, BP 37-1002, Tunis le Belvédère, Tunisia, E-mail: jlassi.zahra@hotmail.fr
[1] ENIT-L.S.E-LR11ES15, University of Tunis EL Manar, BP 37-1002, Tunis le Belvédère, Tunisia
[2] Electrical Engineering Department, Virginia Polytech. Inst. & State University, Blacksburg, VA, USA

transform (HHT) [12], graph theory [13], [14], and self-organizing maps (SOM) [15]. Unlike model-based methods, the measurement-based are independent of model accuracy, with near real implementation readiness using phasor measurement units and without linear approximation. The disadvantage of nonlinear methods based on spectral-graph or intelligent computation is the invisibility and the difficult study of the correspondence between modes and machines.

Recently, a new data-driven nonlinear partitioning technique for power systems has been proposed [16]-[18], based on the spectral analysis of Koopman operator. Applied on snapshots of bus angles, the method enables the decomposition of the system dynamics into single frequency modes. Contrasted to standard harmonic analysis, the Koopman mode (KM) analysis provides, in addition to the full spectrum of linear and nonlinear modes, growing/decaying trajectories that may exist during a transient phase. The identification of the modes and their associated frequencies/growth rates can be formulated as a spectral problem of the Koopman operator. Nonlinear modal coherency yields finer partitioning of power networks. Nonetheless, despite the efficiency of the coherency clustering, the cutsets are determined based solely on graph connectivity. They do not substantiate minimum power-flow disruption and required bands specified in the frequency operating standards. Such scheme does not guarantee stability of the islands since viability requirements are not incorporated in the islands construction process.

In this paper, we propose to construct viable islanding based on KM analysis combined with a subgraph theory. Specifically, an initial partition of the power system is determined based on Koopman nonlinear modal coherency technique applied to bus-angle observable inputs. Over-load and over-generation islands are determined. Pairwise cluster bordering zones are used to generate balancing subgraph candidates. Minimal power mismatch and required dynamic frequency deviation are substantiated within viable islands. If switching actions of constructed balancing subgraphs are not feasible or sufficient for viability requirements, under-frequency load shedding and over-frequency generation shedding schemes are applied. The proposed islanding scheme is applied to the Tunisian 151-bus, 24-machines power system.

2. Koopman Modal Coherency

Coherency identification using Koopman modes analysis has been introduced in [18]. The method characterizes the behavior of nonlinear highly complex dynamics by decomposing them into modes identified from Koopman operator spectral analysis [16]-[18]. Then, it is possible to extract coherent components oscillating with their respective frequencies. The Koopman operator is applied to a dynamical discrete-time system of finite-dimensional space of variables $x \in M$, with nonlinear evolution given by

$$x_{k+1} = f(x_k), \tag{1}$$

where $f(.)$ is a nonlinear function that maps from the manifold M the variables at the instant k to novel variables at instant $k+1$. The Koopman operator U is defined by [16]-[18]

$$Ug(x) = g(f(x)), \tag{2}$$

where $g : M \to \mathbb{R}$ is an observation function denoting a vector of dynamics, such as generators rotors speeds or bus voltages angles measured at different points in a power system. Since the Koopman operator is linear, it satisfies

$$U\varphi_i(x) = \lambda_i\varphi_i(x) \text{ for } i = 1,2,3, \ldots, \quad (3)$$

where $\varphi_i(x)$ is the i^{th} eigenfunction that corresponds to the i^{th} eigenvalue λ_i. If the components of the observation function $g(.)$ lie within the span of Koopman eigenfunctions φ_i, it can be rewritten as

$$g(x_k) = \sum_{i=1}^{\infty} \lambda_i{}^k \varphi_i(x_0)v_i, \quad (4)$$

where the vector-valued coefficients v_i define the Koopman modes. Using an Arnoldi algorithm, approximations to the Koopman eigenvalues and modes may be computed [16]-[18]. Dominant KMs are identified by sorting them based on their growth rates and norms. The growth rate indicates the damping of a KM and the norm quantifies its contribution in the measured data.

Coherency is then defined based on the Koopman modes similarity. For a given j^{th} observable (such as generator speed or bus voltage angle) and a given i^{th} Koopman mode, the amplitude coefficient A_{ij} and the initial phase α_{ij} of the component $v_{ij} = A_{ij}\angle\alpha_{ij}$ are given by [17], [18]

$$A_{ij} = \sqrt{(Re[\varphi_i(x_0)v_i]_j)^2 + (Im[\varphi_i(x_0)v_i]_j)^2} \quad (5)$$

$$\tan \alpha_{ij} = (Im[\varphi_i(x_0)v_i]_j)/\,(Re[\varphi_i(x_0)v_i]_j) \quad (6)$$

A group of observables $O = [1 \ldots p]$ is coherent with respect to a Koopman mode i if the components of this i^{th} mode are similar for all $j \in O$. It is sufficient to verify initial phases for the corresponding mode components to identify phase-coherent dynamics experiencing similar behaviors with respect to that Koopman mode [17]. For a small positive constant ε_α, if two scalar observables j_1 and j_2 satisfy

$$\left|\alpha_{ij_1} - \alpha_{ij_2}\right| < \varepsilon_\alpha, \quad (7)$$

over time, then these two observables are phase-coherent [17], with respect to the phase tolerance ε_α.

3. Subgraph and Connectivity

Topologically, a power network can be represented by a graph $G = (V, E, W)$, where $V(G) = \{v_1, v_2, \ldots, v_N\}$ is the set of its N vertices (buses) and $E = \{e_1, e_2, \ldots, e_L\}$ is its set of L edges (transmission lines). To simulate the power grid, each edge in the graph is assigned a certain weight W such as line admittance or power flow, depending on the targeted application. An edge e_k is a pair (v_i, v_j) that represents a connection between nodes $v_i \in V$ and $v_j \in V$. A graph is connected if there is a path between every pair of vertices. A subset E' of E is called a cutset of G if the deletion of all the edges of E' from G makes G disconnected [19].

The power grid can be analyzed at different topological scales, ranging from single nodes to subsystems, up to the complete system. A subgraph $S_i = (V_i, E_i, W_i)$ of a graph G is a graph which vertex set $V_i(S_i)$ is a subset of the vertex set *V(G),* ($V_i(S_i) \subseteq$V(G)), and which edge set $E_i(S_i)$ is a subset of the edge set E(G),

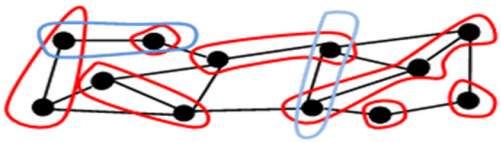

Fig.1. Illustration of disjoint and overlapping subgraphs

(E(S)⊆E(G)). Interconnectivity of subgraphs used in this work assumes that the general graph/network $G = (V, E, W)$ is undirected, unweighted and connected. In order to create a subgraph S_i, it is enough to define a set of vertices V_i and edges E_i, respecting the following rules (i)-(iv). Subgraphs $S_i = (V_i, E_i, W_i)$ can be defined such that [19]

(i) $V_i \subseteq$V;

(ii) $V_i \neq \emptyset$;

(iii) $(v_i, v_j) \in E_i$ if and only if $v_i, v_j \in V_i$, and $(v_i, v_j) \in E$;

(iv) G_i is a connected component.

A valid V_i is a non-empty subset of V that results in a connected component (rule (iv)) not sharing any nodes or edges with other subgraphs (rules (ii) and (iii)). Depending on the application, the constructed subgraphs may be disjoint where $V_i \cap V_j = \emptyset$, otherwise they are overlapping, as illustrated in Fig. 1.

4. Principle Requirements of Islands

The basic requirements for power system islanding pertain to the operational stability in voltage and frequency of the subsystem, taking into consideration its remaining generation inertia, active power reserves, and energy balance capabilities:

4.1. Coherency

An essential step in constructing islands of a power system is coherency among generators and buses within an island. Being modal dependent, coherency means similar dynamics with respect to frequency swings. With regard to coherent initial phases of KMs satisfying (7), the dominant modes are identified and nonlinear coherent bus groups including coherent generators are determined with respect to these modes.

4.2. Frequency control within islands

Frequency, inertia, reserves, and active power balancing are closely coupled parameters. The control of frequency sets up requirements on these parameters:

1) Inertia: Power islands with high inertia can resist large changes in frequency arising from a contingency that leads to an imbalance in supply and demand. Lower levels of inertia increase the susceptibility of the system to rapid changes in frequency because of such an imbalance.

2) Power balancing: The formed islands should be able to preserve generation-load balance. The mismatch should be minimized to a threshold *d,* valued for each island k

$$\left|\sum_{i=1}^{N_{Bk}}(P_{Gi} - P_{Li})\right| \leq d, \tag{8}$$

3) Active reserves: Requirements on generation control and/or load shedding in each island may be expressed by the following inequalities [20], [21]

$$\sum_{i=1}^{N_{Gk}} R_i^{down} \geq \sum_{i=1}^{N_{Bk}} (P_{Gi} - P_{Li}) > 0, \tag{9}$$

$$\sum_{i=1}^{N_{Gk}} \left(R_i^{up} + P_{LSi}\right) \geq \sum_{i=1}^{N_{Bk}} (P_{Li} - P_{Gi}) > 0, \tag{10}$$

where R_i^{up} and R_i^{down} stand for the controllable generation reserve capacities at generator i, deployed for generation increase or decrease respectively.P_{LSi}, P_{Gi} and P_{Li} are the load shedding capacity, the active power generation and load at bus i, respectively. N_{Gk} and N_{Bk} respectively represent the total number of generators and buses in the k^{th} island. The requirement in (9) indicates the island's ability to maintain an active power balance in the case of over-generation, and the requirement in (10) indicates the case of over-load islands.

As island operation is generally an unfavorable emergency condition, smoother requirements on frequency thresholds are allowed. Formally, we have

$$|\Delta f| = |f_{max} - f_n| < \varepsilon, \tag{11}$$

where $\varepsilon = 800\, mHz$, f_n is the nominal frequency, and f_{max} is the maximum dynamic frequency [22]. The frequency of each identified coherent cluster must satisfy prescribed frequency limits $(49{,}2Hz < f < 50{,}8Hz)$ [22].

5. Proposed Islanding Scheme

The k-mean technique is applied on a KM-coherency matrix constructed for the dominant KM phase angles as

$$[K]_{N_o \times N_d} = \begin{bmatrix} \alpha_{11} & \dots & \alpha_{1j} & \dots & \alpha_{1N_d} \\ \vdots & \ddots & \vdots & \ddots & \vdots \\ \alpha_{i1} & \dots & \alpha_{ij} & \dots & \alpha_{iN_d} \\ \vdots & \ddots & \vdots & \ddots & \vdots \\ \alpha_{N_o1} & \dots & \alpha_{N_oj} & \dots & \alpha_{N_oN_d} \end{bmatrix}, \tag{12}$$

where N_o is the number of observables and N_d is the number of dominant KMs. Hence, an initial partitioning of the power system is obtained, with cutsets obtained solely from graph connectivity principle, with a unit weights assigned to all edges. Such scheme does not assure power balancing since static requirements for viability are not incorporated in the islands construction process.

The proposed scheme relies on the reconfiguration of the initial constructed islands, by intervening boundary zones of neighboring clusters as follows:

5.1. Cluster boundary zones

Buses within a cluster feature similarity properties, and similarity is generally evaluated using the notion of distance between data points. Clustering techniques maximize intra-cluster similarities and minimize inter-cluster similarities.

Let $U = \{B_n / n = 1, \dots, N\}$ be a given data set partitioned into N_c clusters, the i^{th} cluster denoted by U_i and its centroid denoted by C_i, $i = 1{,}2, \dots, N_c$. For each data point B_n, let d_{B_n,C_i} be the distance between itself and the centroid C_i of cluster U_i. In the present case, the input data contains the initial phases of the dominant KMs, thus the distance d_{B_n,C_i} is simply given by

$$d_{B_n,C_i} = \left|\alpha_{C_i} - \alpha_{B_n}\right|. \tag{13}$$

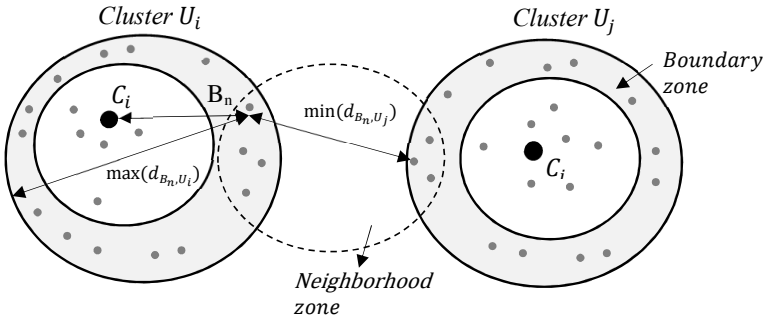

Fig. 2. Illustration of boundary and neighborhood zones

A bus B_n belongs to the i^{th}cluster, if its distance to the i^{th}cluster centroid is the smallest compared to all other $(N_c - 1)$ centroids, that is,

$$d_{B_n,C_i} = min\left(d_{B_n,C_k}\right)_{k=1,\dots,N_c}. \tag{14}$$

A belonging degree of a data point to its cluster is a function of its distance from the centroid, with the highest value given to the closest point. We may define a belonging degree of the data point B_n to its proper cluster U_i as

$$\sigma_{B_n,U_i} = \frac{1}{d_{B_n,C_i} \Big/ min\left(d_{B_j,C_i}\right)_{\substack{j=1,\dots,N_{Ci} \\ B_j \neq C_i}}}. \tag{15}$$

Note that the value of the belonging degree σ_{B_n,U_i} decreases as its distance from the centroid increases. Thus, boundary buses of each cluster feature weaker belonging degrees, which may be delimited by a chosen threshold σ_b, that is,

$$\sigma_{B_n,U_i} \leq \sigma_b. \tag{16}$$

5.2. Cluster neighboring index

Boundary zones of neighboring clusters contain data points satisfying pairwise distance nearness as schematically illustrated in Fig 2. Such property may be quantified by weighing the maximum distance of a bus $B_n \in U_i$ from its inner-cluster buses, to its distance from the nearest bus of a neighboring cluster U_j. For any cluster pair $\left(U_i, U_j\right)$, a neighborhood membership index noted $\eta_{B_{n,ij}}$ is defined for a data point B_n as

$$\eta_{B_{n,ij}} = \frac{\underset{B_k \in U_i}{max}\left(d_{B_n,B_k}\right)_{k=1,\dots,N_{ci}}}{\underset{B_{k'} \in U_j}{min}\left(d_{B_n,B_{k'}}\right)_{k'=1,\dots,N_{cj}}}. \tag{17}$$

The value of $\eta_{B_{n,ij}}$ is highest for buses from U_i featuring nearness to buses from cluster U_j, with unity value occurring when the inner and outer distances in (17) equalize.

5.3. Construction of balancing subgraphs

Upon cluster separation, over-load and over-generation islands are determined from the sign of the dynamic frequency deviations from threshold values (11). An island with centroid C_i, noted $I_{C_i}^0$ is an island satisfying $|\Delta f| < \varepsilon$. Over-load islands have negative Δf, they are noted $I_{C_i}^+$. Over-generation islands denoted $I_{C_i}^-$ have positive Δf. For energy-balancing requirements, neighboring buses may be swapped from over-load islands I^+ to over-generation islands I^-, depending on the connectivity of their associated subgraphs.

First, appropriate sets of buses and subgraphs are defined as follows:
(i) Set of bordering buses: For each cluster, boundary buses are those with lower belonging degrees:

$$B^{0,+,-} = \left\{B_n \in I_{C_i}^{0,+,-} / \sigma_{B_n,U_i} \ll 1\right\}_{\substack{n=1,\dots,N_{Ci} \\ i=1,\dots,N_C}}. \quad (18)$$

(ii) Candidate set of balancing buses: These sets are *k*-combinatorial subsets of B^+ and *k'*-combinatorial subsets of B^-, of cardinals *k* and *k'* respectively:

$$S^+ = \{A \subset B^+ / Card(A) = k; k = 1, \dots, N_B^+\}; \quad (19)$$

$$S^- = \{A \subset B^- / Card(A) = k'; k' = 1, \dots, N_B^-\}. \quad (20)$$

The cardinals of S^+ and S^- are limited by the binomial coefficients given respectively by $C_k^{N_B^+} = \frac{N_B^+!}{(N_B^+ - k)!}$ and $C_{k'}^{N_B^-} = \frac{N_B^-!}{(N_B^- - k')!}$, where N_B^+ and N_B^- represent respectively the number of B^+ and B^- bordering buses.
(iii) Energy balancing subgraphs: Balancing subgraph candidates with vertices constructed from the balancing set of buses S^+ and S^- which feature intra-connectivity, and connectivity respectively with islands I^+ and I^-, that is,

$$S_{G_{Bal}}^+ = \{G(V,E)/V \subset S^+ \; and \; (G \cup S^-) \; is \; connected\}; \quad (21)$$

$$S_{G_{Bal}}^- = \{G(V,E)/V \subset S^- \; and \; (G \cup S^+) \; is \; connected\}. \quad (22)$$

We can see that the balancing subgraph candidates may be overlapping, since they are formed from the balancing set of buses, which is combinatorial.

5.4. Islanding scheme

The proposed islanding scheme combines the Koopman based coherency partition, complemented by the following algorithm summarized in the bloc diagram of Fig.3:
(i) Initial islanding: Firstly, based on bus-voltage angles as observable inputs, the Koopman modes are computed. Dominant ones with largest norms and growth rates are determined. The coherency matrix (12) is constructed. By applying the *k*-means clustering technique for the dominant modes, an initial KMA based islanding is proposed.
(ii) *Viability requirements check*: Viability requirements for short term operation in frequency are assessed: power mismatch, frequency deviation.
(iii) *Island modulation*: Energy balancing subgraphs are constructed to modulate islands so that minimum viability requirements are satisfied. Subgraphs belonging to $S_{G_{Bal}}^+$ constructed from over-load islands, may be switched to an over-generation island I^-.

In search for minimum power mismatch, a swapping action may apply where subgraphs belonging to $S_{G_{Bal}}^+$ switch to an over-generation island I^-, and simultaneously, subgraphs belonging to the over-generation balancing set $S_{G_{Bal}}^-$ may switch to an island I^+. This is performed in a systematic search algorithm where each element of $S_{G_{Bal}}^+$ is paired with each element of $S_{G_{Bal}}^-$, making up the Cartesian product set $S_{G_{Bal}}^+ \times S_{G_{Bal}}^-$comprising all ordered pairs of subgraph elements from $S_{G_{Bal}}^+$ and $S_{G_{Bal}}^-$ as defined in Table 2. Each balancing subgraph candidate is tested in search for minimum power mismatch in its associated islands. In such case, connectivity testing for a subgraph pair $(G_{k'}^-, G_k^+)$ requires the connectivity of : $(G_k^+ \cup I^-)$ and $(G_{k'}^- \cup I^+)$.

(iv) *Load and/or generation shedding*: If island reconfiguration was not sufficient for viability requirements, a load shedding or generation shedding will be applied in this island.

Table 2: Ordered Pairs of Balancing Subgraphs

$S^{-}_{G_{Bal}}$ \ $S^{+}_{G_{Bal}}$	G_1^+	...	G_k^+	...	$G_{N_B^+}^+$
G_1^-	(G_1^-, G_1^+)	...	(G_1^-, G_k^+)	...	$\left(G_1^-, G_{N_B^+}^+\right)$
⋮	⋮	...	⋮	...	⋮
$G_{k'}^-$	$(G_{k'}^-, G_1^+)$	...	$(G_{k'}^-, G_k^+)$	...	$\left(G_{k'}^-, G_{N_B^+}^+\right)$
⋮	...	...	...	...	...
$G_{N_B^-}^-$	$\left(G_{N_B^-}^-, G_1^+\right)$	...	$\left(G_{N_B^-}^-, G_k^+\right)$	...	$\left(G_{N_B^-}^-, G_{N_B^+}^+\right)$

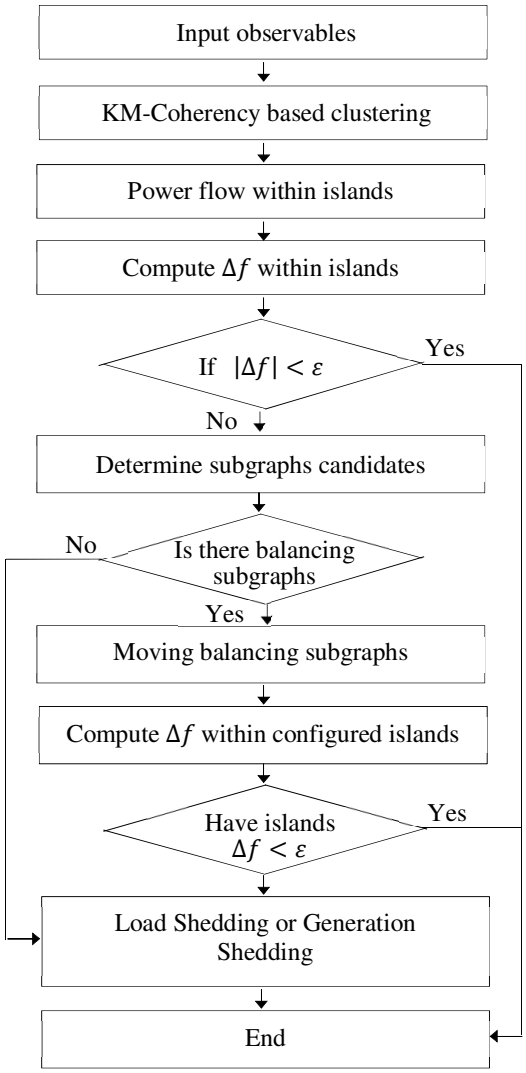

Fig. 3. Proposed islanding scheme

6. Simulation Results

6.1. Study case description

The proposed islanding scheme is applied to a large scale power system: The Tunisian power system consists of 151-buses and 24-machines, with a total generation capacity of

3000 MW. The generators are equipped with speed and voltage regulators, they may be geographically grouped into three main groups: North, Center and South, comprising respectively 12, 5, and 7 machines. The KMA procedure is applied on sampled dynamics of bus voltage angles following a three-phase short-circuit applied in the North at bus N°116 RADES-CC at time t=1s, of duration 250 ms. Simulations are performed using the software Power System Simulator for Engineering (PSS/E) [23]. The system data are given in the Appendix.

6.2. KM based coherency

Following the applied disturbance, bus voltage angles and generators rotor speed responses exhibited oscillatory responses as depicted in Fig.4. Coherency is noted both in generator swing dynamics, and in bus voltage angles, within groups in the northern, central, and southern regions of the system. Six dominant Koopman modes noted KM-1 through KM-6, are identified with frequencies worth 0.04 Hz, 0.1 Hz, 0.25 Hz, 0.21 Hz, 0.15 Hz and 0.71 Hz, respectively.

For the first five modes, all voltage phases are closely grouped around their respective centroids, as depicted in Fig. 5. Hence, the system is not partitioned. Nonetheless, for KM-6 of frequency 0.71 Hz, the phase angles are clustered around three centroids, yielding three coherent bus groups as depicted in Fig. 6. These groups correspond to Northern, Central, and Southern regions of the system. As the retained grouping should be valid for all identified dominant KM modes, the intersection of the partitions is retained. Thus, the 3 group clustering named North, Center, South identified by KM-6 is retained.

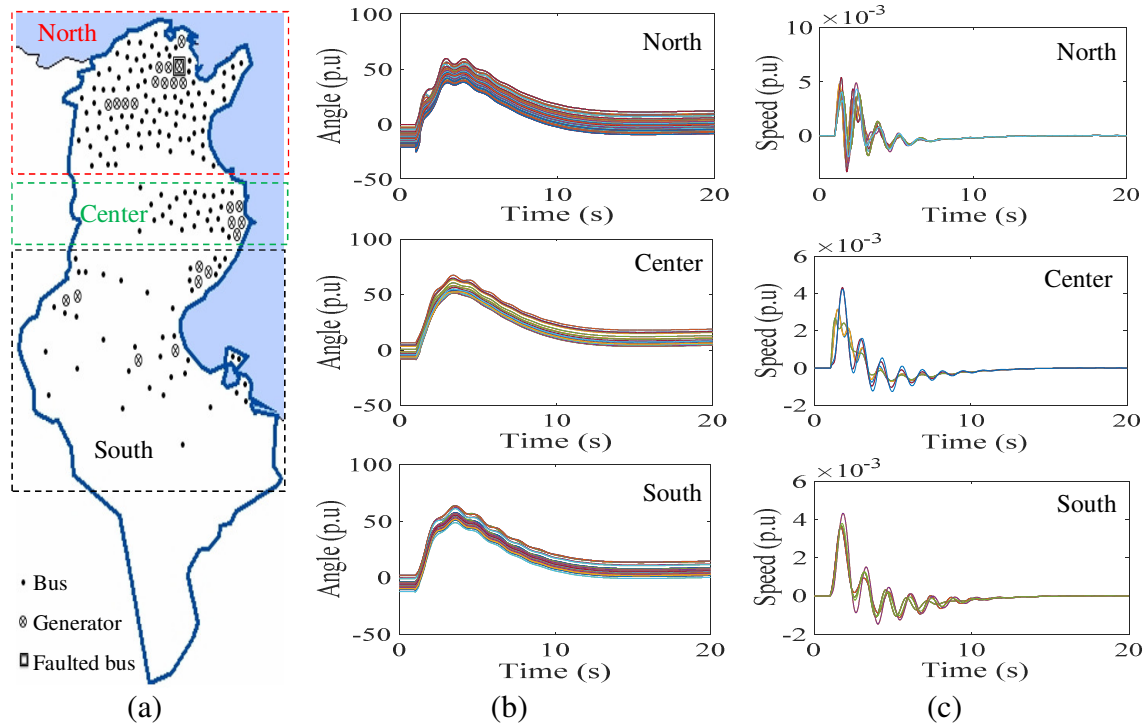

Fig.4. Power system variations following the disturbance. (a) Power system structure. (b) Bus voltage angles. (c) Generator rotor angle speeds.

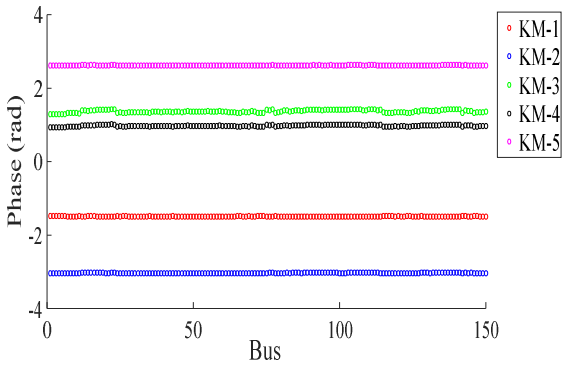

Fig.5. Bus coherency results for the dominant KM-1,2,3,4,5

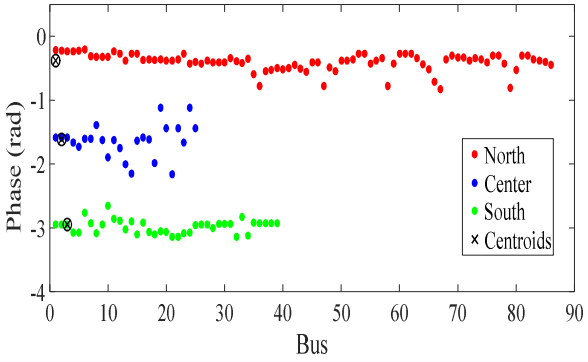

Fig. 6. Bus coherency results for the dominant KM-6

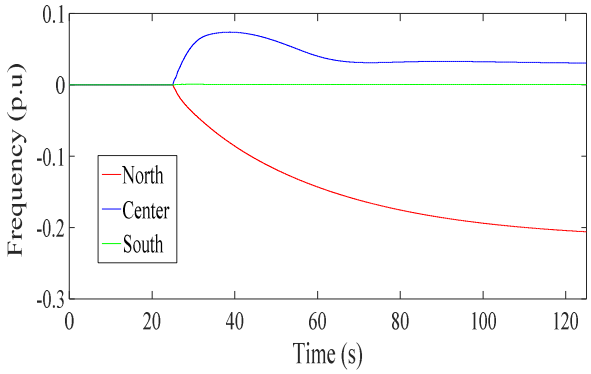

Fig. 7. Frequency responses to initial islanding based on KM coherency

Table 3: Ordered Power and Frequency Violations of Islands using KM Coherency

	North	Center	South
Generator N°	111-112-113-114-115-116-117-141-142-143-144-183	513-514-515-516-517	623-624-625-753-754-810-823
Generation (MW)	1350	870	825
Power mismatch (MW)	291.4	322	14.55
Frequency deviation (Hz)	10	3.75	0.05

This initial power system partitioning based solely on Koopman modal coherency is evaluated for dynamic frequency deviations. The frequency responses are depicted in Fig.7, indicating frequency deviations reaching 10 Hz, 3.75 Hz and 0.05 Hz in the North, the Center and the South respectively. Thus, the identified northern island is an over-load island, the central island is an over-generation island and the southern island is a viable island. Power flow results are summarized in Table 3, valuing the resulting power mismatch of the islanded regions

6.3. Islanding modulation

In order to reach the required bands specified in the frequency operating standards [20] for the two nonviable islands, an islanding reconfiguration is applied. To modulate the clusters for energy balance, boundary zones of the northern and central islands are determined for the dominant mode KM-6. Figures 8 and 9 show the distances to centroid

and cluster belonging degrees for buses in the northern and central islands, respectively. It is noted that a number of buses located on the northern boundaries have belonging degrees lower than 0.03, as shown in Fig. 8. For the central zone, buses located on its boundaries have relatively lower belonging degrees. The chosen belonging degree threshold for this study was about $\sigma_b = 0.03$. Among these boundary buses, those featuring north-center neighbourhood proximity will be used to construct balancing subgraph candidates.

Table 4 summarizes the constructed balancing subgraphs. These subgraphs are systematically constructed from the northern and central boundary buses featuring neighborhood proximity, indicated by their neighborhood membership indices: Six northern buses belong to the northern boundary zone (Fig. 8), and six central buses belong to the central boundary zones (Fig. 10). Thus, the candidate sets of balancing buses are 6-combinatorial subsets of northern boundary buses and 6-combinatorial subsets of central boundary buses. For the over-load island, seven balancing subgraphs with vertices constructed from the balancing northern set of buses, feature inter-connectivity and connectivity with the central island. For the over-generation island, six balancing subgraph candidates are defined.

Table 4: Constructed Balancing Subgraphs

Over-load island subgraphs		Over-generation island subgraphs		Tested subgraphs		Subgraph movement yielding least power mismatch
Total Number	Connected candidates $S^{+}_{G_{Bal}}$	Total Number	Connected candidates $S^{-}_{G_{Bal}}$	Balancing pairs (Total number = 42)	Over-load subgraphs	
C_1^6	$\{B_2^+\};\{B_6^+\}$	C_1^6	$\{B_1^-\};\{B_5^-\}$	$\{B_2^+\}\times S^-_{G_{Bal}}$ $\{B_6^+\}\times S^-_{G_{Bal}}$	$\{B_2^+\}$; $\{B_6^+\}$; $\{B_1^+,B_2^+\}$; $\{B_5^+,B_6^+\}$; $\{B_4^+,B_5^+,B_6^+\}$; $\{B_3^+,B_5^+,B_6^+\}$; $\{B_3^+,B_4^+,B_5^+,B_6^+\}$	$\{B_1^+,B_2^+\}$; $\{B_3^+,B_4^+,B_5^+,B_6^+\}$
C_2^6	$\{B_1^+,B_2^+\}$; $\{B_5^+,B_6^+\}$	C_2^6	$\{B_4^-,B_5^-\}$	$\{B_1^+,B_2^+\}\times S^-_{G_{Bal}}$ $\{B_5^+,B_6^+\}\times S^-_{G_{Bal}}$		
C_3^6	$\{B_4^+,B_5^+,B_6^+\}$; $\{B_3^+,B_5^+,B_6^+\}$	C_3^6	$\{B_3^-,B_4^-,B_5^-\}$	$\{B_4^+,B_5^+,B_6^+\}\times S^-_{G_{Bal}}$ $\{B_3^+,B_5^+,B_6^+\}\times S^-_{G_{Bal}}$		
C_4^6	$\{B_3^+,B_4^+,B_5^+,B_6^+\}$	C_4^6	$\{B_2^-,B_3^-,B_4^-,B_5^-\}$	$\{B_3^+,B_4^+,B_5^+,B_6^+\}\times S^-_{G_{Bal}}$		
C_5^6	$\emptyset$	C_5^6	$\{B_2^-,B_3^-,B_4^-,B_5^-,B_6^-\}$	$\emptyset$		
C_6^6	$\emptyset$	C_6^6	$\emptyset$	$\emptyset$		

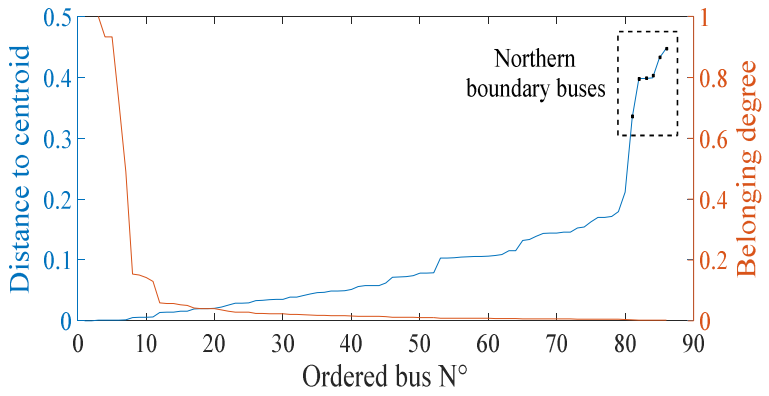

Fig. 8. Distance from centroid and belonging degrees of buses in North island for KM-6

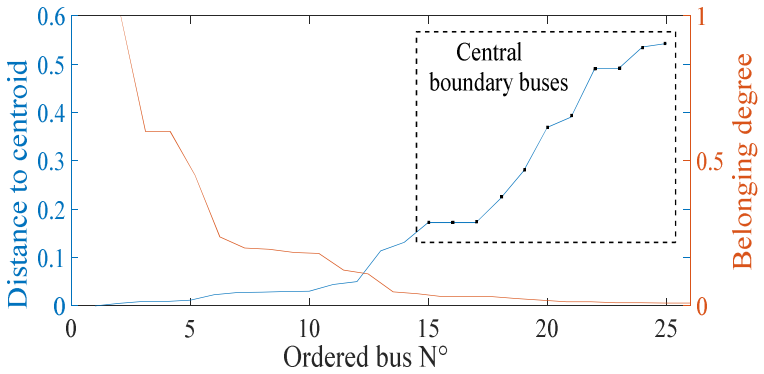

Fig. 9. Distance from centroid and belonging degrees of buses in Center island for KM-6

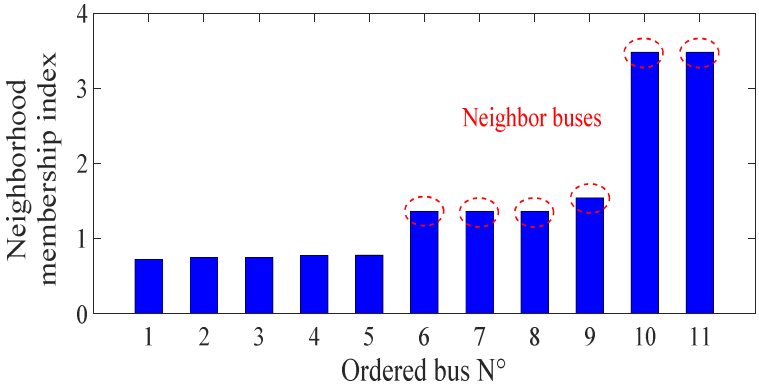

Fig. 10. Neighborhood membership indices of the Center island boundary buses for KM-6

To modulate the Tunisian nonviable islands, nine pairs of subgraphs may be constructed from northern and central subgraph candidates as defined in Table 4. Each northern over-load subgraph candidate and each balancing pair of subgraphs are tested in search for minimum power mismatch. Swapping action for each constructed balancing pair is applied. Switching action for each constructed over-load subgraph candidate is applied. Power mismatch within the over-generation island is computed for each switching case and each swapping case. The switching action of two over-load subgraphs belonging to the northern island led to the least power mismatch in the central island as indicated in Table 4. The first one contains two connected northern boundary buses and the second one contains the other four northern boundary buses.

The results demonstrate that moving the six northern boundaries buses to the central island reduces the central dynamic frequency deviation from 3.75 Hz to 2.5 Hz, and reduces the northern dynamic frequency deviation from 10 Hz to 2.2 Hz as shown in Fig. 11. Thus, the balancing scheme was not sufficient to realize viable northern and central islands with acceptable frequency deviations. Therefore, a load shedding for the northern island and a generation shedding for the central island are needed, as complementary corrective actions.

Accordingly, a generation shedding of 200 MW in the configured central island is applied, corresponding to the generation of two central machines (G513 and G514). A load shedding of 115 MW is applied to the configured northern island. These shedding actions have brought the dynamic frequency deviation to the required frequency band as shown in Fig. 12. Table 5 compares the amount of power shed using the KM based islanding, and the KM-subgraph scheme. The latter achieved a reduction in the amount of load and generation shedding to reach the required bands specified in the frequency operating standards [22].

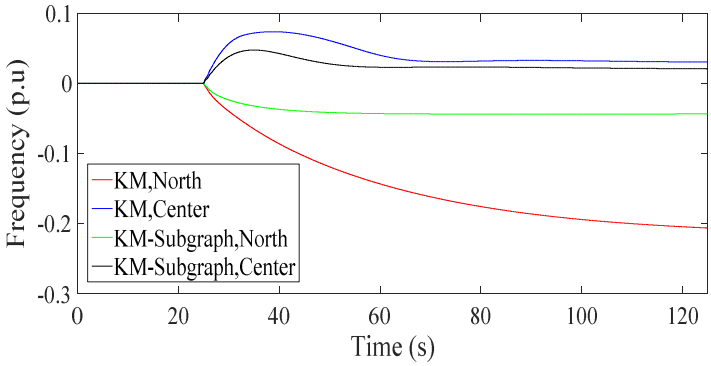

Fig. 11. Comparison of frequency responses of the KM and KM-subgraph islanding methods without load shedding application

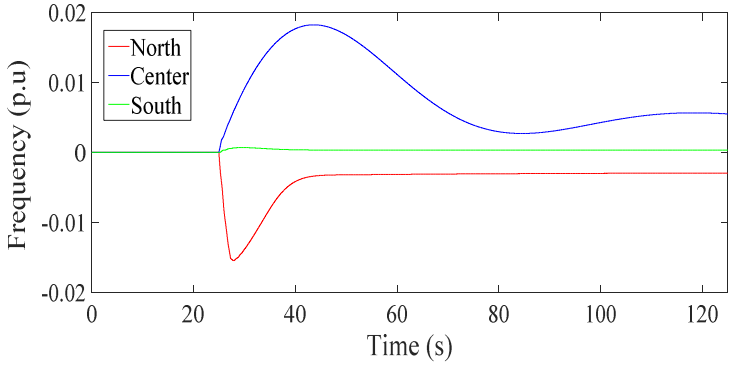

Fig. 12. Frequency responses using the KM-subgraph islanding scheme with load shedding application

Table 5: Load/Generation Shedding Results

Method / Control action	KM method		KM-Subgraph	
	Island	**Amount (MW)**	**Island**	**Amount (MW)**
Load shed	North	249	North	115
Generation Shed	Center	280	Center	200

7. Conclusion

This paper proposed a new methodology for power system islanding based on Koopman modal coherency, combined with subgraph technique. Balancing subgraph candidates are searched for via a systematic search algorithm, and switching actions from over-load subgraphs to neighboring over-generation subgraphs are performed. If these corrective actions are not feasible or not sufficient to guarantee viable islands, load shedding and/or generation shedding actions are initiated. As a real system application of the proposed islanding scheme, a dataset from the Tunisian power system was analyzed.

The advantages of the proposed methodology include the following:

- Compared to standard graph-based clustering methods where all system buses are considered, the subgraphs of the proposed method involve only limited numbers of buses, namely bordering ones.
- Subgraphs are constructed solely from weaker belonging buses, thus the KM coherency clustering and associated centroids are least affected.

- The proposed islanding method assures nonlinear coherency provided by the KMC algorithm and optimizes viability of constructed islands using the balancing subgraph candidates, via a systematic search algorithm.
- Subgraph swapping for power mismatch corrections are performed while preserving the nonlinear coherency properties of islands, which favors their viability under subsequent large events.
- The amount of load or generation shed may be minimized.

The proposed approach can be used at planning stage by the system operator to generate candidate islanding which may be analyzed in detail for stability aspects with dynamic simulation.

References

[1] A. Esmaeilian and M. Kezunovic, "Prevention of Power Grid Blackouts Using Intentional Islanding Scheme," *IEEE Trans. Ind. Appl.*, vol. 53, no. 1, pp. 622-629, 2017.

[2] A. N. Ab Salam, H. Mohamad, N. Y. Dahlan, and S. Raza, "Performance of Multiple Passive Islanding Detection Technique for Synchronous Type of DG", *J. Electrical Systems*, vol. 13, no. 3, pp. 568-578, 2017.

[3] Ch. Rami Reddy, K. Harinadha Reddy, "Islanding detection for inverter based distributed generation with Low frequency current harmonic injection through Q controller and ROCOF analysis", *J. Electrical Systems*, vol. 14, no. 2, pp. 179-191, 2018.

[4] S. Raza, H. Mokhlis, H. Arof, J.A. Laghari, and L. Wang, "Application of signal processing techniques for islanding detection of distributed generation in distribution network: A review," *Energy Convers. Manag.*, vol. 96, pp. 613-624, 2015.

[5] M. H. Haque and A. H. M. A. Rahim, "Identification of coherent generators using energy function," *IEE Proceedings*, Part C, vol. 137,no. 4, pp. 255-260, July 1990.

[6] G. Xu and V. Vittal, "Slow Coherency Based Cutset Determination Algorithm for Large Power Systems," *IEEE Trans. Power Syst.,* vol. 25, no. 2, May 2010.

[7] M. Mahdi and V. M. I. Genc, "A security assessment for slow coherency based defensive islanding," *Proc. IEEE* 9th International *Conference on Electr and Electronics Eng*, Bursa, Turkey, Nov. 2015.

[8] V.L. Merlin, R.C. Santos, A.P. Grilo, J.C.M. Vieira, D.V. Coury, and M. Oleskovicz, "A new artificial neural network based method for islanding detection of distributed generators," *Int. J. Electr. Power Energy Syst*., vol. 75, pp. 139-151, 2016.

[9] D. Kumar and P. S. Bhowmik, "Artificial neural network and phasor data-based islanding detection in smart grid," *IET Gener. Transm. Distrib*., vol. 12, no. 21, September 2018.

[10] X. Liu, D. M. Laverty, R. J. Best, K. Li, D. J. Morrow, and S. McLoone, "Principal Component Analysis of Wide-Area Phasor Measurements for Islanding Detection—A Geometric View," *IEEE Trans. Power Del.*, vol. 30, no. 2, pp. 976-985, April 2015.

[11] M. Davodi, H.-R. Modares, E. Reihani, and A. Sarikhani, "Coherency approach by hybrid PSO, K-Means clustering method in power sys," *Proc. IEEE 2nd Int. Power and Energy Conf.*, pp. 1203- 1207, 2008.

[12] M. Mishra, M. Sahani, and P.K. Rout, "An islanding detection algorithm for distributed generation based on Hilbert-Huang transform and extreme learning machine," *Sustainable Energy, Grids and Networks*, vol. 9, pp. 13-26, March 2017.

[13] O. Gomez and M.A. Rios, "Real time identification of coherent groups for controlled islanding based on graph theory," *IET Gen., Trans. & Dist.*, vol. 9, no. 8, pp. 748-758, May 2015.

[14] J. Quirós-Tortós, R. Sánchez-García, J. Brodzki, J. Bialek and V. Terzija, "Constrained spectral clustering-based methodology for intentional controlled islanding of large-scale power systems," *IET Gen., Trans. & Dist.*, vol. 9, no. 1, pp. 31-42, Jan. 2015.

[15] M. Mahdi and I. Genc, "Defensive islanding using self-organizing maps neural networks and hierarchical clustering," *in Proc. IEEE Eindhoven Power Tech*, Eindhoven, Netherlands, 2015.

[16] Y. Susuki, I. Mezic, F. Raak, and T. Hikihara, "Applied Koopman operator theory for power systems technology, Nonlinear Theory and Its Applications," *IEICE*, vol. 7, no. 4, pp. 430-459, 2016.

[17] F. Raak, Y. Susuki, and T. Hikihara, , "Data-Driven Partitioning of Power Networks via nonlinear Koopman Mode Analysis," *IEEE Trans. Power Syst.*, vol. 31, no. 4, pp. 2799-2808, 2015.

[18] Y. Susuki and I. Mezic, "Nonlinear Koopman modes and coherency identification of coupled swing dynamics," *IEEE Trans. Power Syst.*, vol. 26, no. 4, pp. 1894-1904, 2011.

[19] L. Antiqueira and L. da Fontoura Costa, "Characterization of Subgraphs Relationships and Distribution in Complex Networks," *New Journal of Physics*, vol. 11, no. 1, pp. 34, 2009.

[20] J.J. Ford, H. Bevrani, and G. Ledwich, "Adaptive load shedding and regional protection," *Int. J. Electr. Power Energy Syst*., vol. 31, pp. 611-618, 2009.

[21] F. Xu and X.F. Wang, "Determination of load shedding to provide voltage stability," *Int. J. Electr. Power Energy Syst*., vol. 33, pp. 515-521, 2011.
[22] Operation Handbook, UCTE, 2004.
[23] PSS®E 33.4 Model Library, Siemens Industry, Inc. Siemens Power Technologies International March, 2013.

Acknowledgment

This research is a cooperative framework between the National Engineering school of Tunis (ENIT) and the Tunisian Electricity and Gas Company (STEG). The authors are grateful to National Energy Control Center team for providing the Tunisian power system data to support this paper.

Appendix

Table A1: Frequency Deviations Standards for Nominal Frequency 50Hz [22]

Code	Criteria	$\Delta f\ (mHz)$
C2.1.	Calling up of Primary Control	± 20
C2.2.	Maximum Quasi-Steady-State	± 180
C2.3.	Minimum Dynamic Frequency Deviation	-800
C2.4.	Load-Shedding Frequency Criterion	Between -1000 and -2500
C2.5.	Maximum Dynamic Frequency Deviation	$+800$

Table A2: System Generators Data

Bus N°	Bus name	Nominal power (MW)	Power rating (MVA)	Voltage rating (kV)	Exciter Model	Turbine Governor Model
111	RADESV1	160	212.5	15.5	IEEEX1	IEEEG1
112	RADESV2	160	212.5	15.5	IEEEX1	IEEEG1
113	RADESV3	160	212.5	15.5	IEEET1	IEEEG1
114	RADESV4	160	212.5	15.5	IEEET1	IEEEG1
115	RDSIIG1	140.5	165.3	15.5	IEEX2A	GAST2A
116	RDSIICC	258	303	18	IEEX2A	IEEEG1
117	RDSIIG2	140.5	165.3	15.5	IEEX2A	GAST2A
141	BMCTG1	120	147.63	15.5	EXAC2	GAST2A
142	BMCTG2	120	147.63	15.5	EXAC2	GAST2A
143	BMCTG3	120	147.63	15.5	EXAC2	GAST2A
144	BMCTG4	120	147.63	15.5	EXAC2	GAST2A
183	GOULETG	120	150	15.5	IEEEX1	GAST2A
513	SOUSSEG1	120	147.63	15.5	EXBAS	GAST2A
514	SOUSSEG2	120	147.63	15.5	EXBAS	GAST2A
515	SOUSSECC	120	159.63	15.5	EXBAS	IEESGO
516	CC_C_SSE	440	470	20	ESST1A	IEEEG1
517	CC_D_SSE	440	470	20	ESST1A	IEEEG1
623	THY_TG1	120	147.63	14	IEEEX1	GAST2A
624	THY_TG2	120	147.63	14	IEEEX1	GAST2A
625	THY_TG3	120	147.63	14	IEEEX1	GAST2A
753	FERIATG1	120	147.63	14	IEEEX1	GAST2A
754	FERIATG2	120	147.63	14	IEEEX1	GAST2A
810	GHNCC	425	500	21	ST5B	IEEEG1
823	BOUCHTG3	120	147.63	15.5	EXAC2	GAST2A